Published in final edited form as:

Curr Protoc Cytom. ; 83: 12.9.1–12.9.25. doi:10.1002/cpcy.32.

Live-Animal Imaging of Renal Function by Multiphoton Microscopy

Kenneth W. Dunn[1], **Timothy A. Sutton**[1], and **Ruben M. Sandoval**[1]

[1]Indiana University School of Medicine, Indianapolis, Indiana

Abstract

Intravital microscopy, microscopy of living animals, is a powerful research technique that combines the resolution and sensitivity found in microscopic studies of cultured cells with the relevance and systemic influences of cells in the context of the intact animal. The power of intravital microscopy has recently been extended with the development of multiphoton fluorescence microscopy systems capable of collecting optical sections from deep within the kidney at subcellular resolution, supporting high-resolution characterizations of the structure and function of glomeruli, tubules, and vasculature in the living kidney. Fluorescent probes are administered to an anesthetized, surgically prepared animal, followed by image acquisition for up to 3 hr. Images are transferred via a high-speed network to specialized computer systems for digital image analysis. This general approach can be used with different combinations of fluorescent probes to evaluate processes such as glomerular permeability, proximal tubule endocytosis, microvascular flow, vascular permeability, mitochondrial function, and cellular apoptosis/necrosis.

Keywords

Multiphoton microscopy; intravital microscopy; *in vivo* microscopy; fluorescence microscopy

INTRODUCTION

Intravital microscopy, microscopy of living animals, is a powerful research technique that combines the resolution and sensitivity found in microscopic studies of cultured cells with the relevance and systemic influences of cells in the context of the intact animal. Intravital microscopy has been applied to renal research for over 100 years, having first been used to observe the function of the kidney of a living mouse in 1912 (Ghiron, 1912, and see review in Steinhausen and Tanner, 1976). Since that time, investigators have exploited that ability to observe blood flow and tubular function at the cortical surface to better understand kidney function under normal and pathological conditions. The power of intravital microscopy has recently been extended with the development of multiphoton fluorescence microscopy systems. These systems are capable of collecting optical sections from deep within the kidney at subcellular resolution, supporting high-resolution characterizations of the structure and function of glomeruli, tubules, and vasculature in the living kidney.

Intravital microscopy requires a combination of unique skills and specialized equipment. Studies require technicians skilled in microscopy as well as in animal handling, including

surgery. Studies require facilities for animal housing and surgery, microscope systems equipped with systems for maintenance and monitoring of living animals, and computer systems equipped with image-analysis software.

The kidney is particularly amenable to intravital microscopy since many of its most important functions and physiological can be addressed using fluorescent probes introduced into the vasculature. A typical study begins with the preparation of fluorescent probes, followed by anesthesia, surgical preparation, and mounting of the animal on the stage of the microscope system. Fluorescent probes are administered to the animal, followed by image acquisition for a period of up to 3 hr. In many cases, the animal is then euthanized, or in the case of survival surgery techniques, the animal may be surgically closed and allowed to recuperate. Images are transferred via a high-speed network to specialized computer systems for digital image analysis.

As described below, this general approach can be used with different combinations of fluorescent probes to simultaneously evaluate processes such as glomerular permeability, proximal tubule endocytosis, microvascular flow, vascular permeability, mitochondrial function, and cellular apoptosis/necrosis. Procedures are written for studies of rats, but most are equally appropriate to studies of mice as weight-proportional probe dosages are similar for rats and mice. The procedures described here are written for studies in which imaging is to be conducted at a single time point. For a description of an approach that supports longitudinal imaging of the same animal over days or weeks, we refer the reader to an indwelling imaging window system developed by the laboratory of Jacco van Rheenan. The assays described here are equally applicable using this window system.

BASIC PROTOCOL 1 GLOMERULAR PERMEABILITY

In the absence of experimental manipulations (e.g., hydronephrosis), the glomeruli of most strains of mice and rats are positioned far enough below the capsule that few are accessible to microscopic analysis. However, a significant fraction of the glomeruli of two strains of rats, the Munich Wistar Frömter and Simonsen strains, are sufficiently superficial that they support microscopic analysis of the capillary loops and Bowman’s space of individual glomeruli. Munich Wistar Frömter rats differ from the Simonsen strain in that they have a greater number of superficial glomeruli and a slightly lower glomerular sieving coefficient (GSC) for albumin (Sandoval et al., 2012). The process of glomerular filtration is apparent in the intravital image shown in Figure 1. This figure shows a multiphoton optical section of the kidney of a rat injected with Hoechst 33342 to label nuclei (blue), a 500-Kda dextran–Alexa 488 (green) that is retained in the vasculature, and a 5-Kda dextran-rhodamine (red) that is rapidly filtered, appearing first in the Bowman’s space (center), then in the proximal tubules (top), and finally concentrating in the distal tubules (bottom left). For evaluation of altered glomerular permeability, a probe closer to threshold size of permeability, such as a 40,000-Da dextran, will provide a more sensitive indicator. The approach described below was used to demonstrate that 30 to 50 times more albumin is filtered by the glomerulus than previously determined using micropuncture and fractional clearance (Russo et al., 2007).

Materials (per Support Protocol)

Munich Wistar Frömter rat

70,000-Da dextran–Alexa 488

40,000-Da dextran-rhodamine

Isotonic saline, sterile

Hoechst 33342

Additional reagents and equipment for animal preparation

Experimental preparations (per Support Protocol)

1. Surgically prepare the animal.
2. Prepare a mixture of 70,000-Da dextran–Alexa 488 and 40,000-Da dextran-rhodamine (for a dose of 1 mg/kg of each in 0.5 ml sterile, isotonic saline).
3. Aliquot Hoechst 33342 solution (for a dose of 1 mg/kg in 0.5-ml of sterile, isotonic saline).
4. Prepare the microscope. Set laser illumination to 800 nm. Based upon settings determined in similar previous studies, adjust the laser power and detectors such that anticipated maximum signals in the two channels are similar, and below saturation. Set detector offset such that a slightly positive signal is obtained from an empty field.

Experimental approach

1. Inject Hoechst 33342 intravenously. Collect images in blue, red, and green channels.

   Images collected in red and green channels will serve as “background” images.
2. After ~10 min, find a suitable glomerulus for analysis. Ensure that the animal and the field are stable.
3. Rapidly inject 70,000-Da dextran–Alexa 488 and 40,000-Da dextran-rhodamine solution intravenously.
4. Starting immediately after injection, collect images of the glomerulus every second for a period of 2 min.

Data analysis

Determine the permeability of the 40,000-Da relative to that of the 70,000-Da dextran by measuring, at each point in time, the fluorescence of each in the capillaries and Bowman’s space of the glomerulus. These quantities can then be expressed as a “generalized polarity” measurement that varies from +1 to −1 (Yu et al., 2005), by the following equation:

$$GP=(\mathrm{I}_{70\mathrm{kDa}}-\mathrm{I}_{40\mathrm{kDa}})/(\mathrm{I}_{70\mathrm{kDa}}+\mathrm{I}_{40\mathrm{kDa}})$$

Where I = the measured signal intensity minus the background, as measured in the corresponding channel of the background images. The relative glomerular permeability is then measured as the difference between the GP measured in the glomerulus and that measured in the original solution.

Alternatively, the permeability of a single glomerulus may be also be quantified from the relative fluorescence of a single, freely filtered probe in the capillaries versus the Bowman's space under conditions of constant probe infusion. The authors have found that this technique yields results nearly identical to those obtained through equilibrium dialysis (Tanner et al., 2004; Russo et al., 2007).

Subsequent studies from our lab have demonstrated that measurements of GSC critically depend upon accurate estimates of background levels (Sandoval et al., 2014, Sandoval and Molitoris, 2014). While it might seem appropriate to adjust detector offset such that pixel values of zero are obtained in the absence of fluorescent probes (Schiessl and Castrop, 2013, Schiessl et al., 2015), such aggressive adjustment of detector offset not only eliminates detection of dim fluorescence, but it also artificially depresses estimates of fluorescence background, resulting in erroneously low measures of GSC. Accurate measures of GSC depend upon adjustment of detector offset such that positive values are obtained in regions lacking fluorescent probe, so that background levels are estimated of means of a distribution of pixel values that haven't been artificially truncated to zero during the collection process. It is critical to maintain identical settings for the duration of the experiment to assure proper sensitivity and background correction. A more complete description of the glomerular permeability assay was published in an online tutorial video (Sandoval and Molitoris, 2013).

BASIC PROTOCOL 2 PROXIMAL TUBULE ENDOCYTOSIS

One of the primary functions of the renal proximal tubules is to scavenge small- to medium-sized, biologically important compounds that are filtered before their loss to urinary excretion, through the process of endocytosis. Intravital multiphoton microscopy is capable of detecting uptake of luminal filtrate into individual endosomes, and to quantify endocytic uptake. This approach has recently been used to illuminate unforeseen aspects of albumin transport in the kidney.

However, intravital studies demonstrated that nearly all of the filtered albumin is rapidly and effectively reclaimed via endocytosis by proximal tubule cells, particularly in the S1 segment (Russo, Sandoval et al. 2007). An example of the use of fluorescent dextrans to characterize proximal tubule endocytosis is shown in Figure 2.

Materials (per Support Protocol)

Animal

3,000-Da dextran–Alexa 488, 10,000-Da dextran-rhodamine or fluorescent bovine serum albumin

Isotonic saline, sterile

Additional reagents and equipment for animal preparation

Experimental preparations (per Support Protocol)

1. Surgically prepare the animal.
2. Prepare dextran or albumin solution (for a dose of 1 mg/kg in 0.5 ml sterile, isotonic saline).
3. Prepare the microscope. Set laser illumination to 800 nm. Based upon settings determined in similar previous studies, adjust the laser power and detectors such that anticipated maximum signals in the two channels are similar, and below saturation. Set detector offset such that a slightly positive signal is obtained from an empty field.

Experimental approach

1. Acquire images of a field of proximal tubule (or multiple fields) prior to infusion of any compound to characterize the autofluorescence associated with the lysosomes of proximal tubules (particularly important if planning quantitative studies).
2. Depending on the study design, infuse fluorescent dextran (or albumin) in 0.5 ml sterile, isotonic saline; be sure to flush the access line with saline to clear compound from the dead space in the line.
3. Collect images of the field (or multiple fields) for up to 1 hr.

   It is important to carefully monitor acquisition parameters for quantitative studies since probes will rapidly accumulate in endosomes and lysosomes, and can result in saturating signal levels.

Data analysis

Quantify endocytic uptake from the increase in punctate endocytic fluorescence (using a median filter to remove background fluorescence) as a function of time in a series of images collected from the same field.

BASIC PROTOCOL 3 VASCULAR FLOW

Peritubular and glomerular blood flow has an intrinsic relationship with tubular function and glomerular filtration, respectively. More than 40 years ago Steinhausen and coworkers (1973) utilized intravital videomicroscopy to examine peritubular blood flow of vessels on the surface of the kidney. The greater imaging depths possible with multiphoton microscopy allows for the study of both glomerular and peritubular vascular blood flow below the surface of the cortex (Sharfuddin, Sandoval et al. 2009, Basile, Friedrich et al. 2011, Ferrell, Sandoval et al. 2015).

Materials (per Support Protocol)

Animal

Fluorescent 500,000-Da dextran (or fluorescent bovine serum albumin)

Isotonic saline, sterile

Additional reagents and equipment for animal preparation

Experimental preparations (per Support Protocol)

1. Surgically prepare the animal.
2. Aliquot fluorescent 500,000-Da dextran (for dose of 10 to 15 mg/kg in 0.5 ml sterile, isotonic saline) or albumin (for a dose of ~1 mg/kg).
3. Prepare the microscope. Set laser illumination to 800 nm. Based upon settings determined in similar previous studies, adjust the laser power and detectors such that anticipated maximum signals are below saturation. Set detector offset such that a slightly positive signal is obtained from an empty field.

Experimental approach

1. Inject fluorescently-labeled 500,000-Da dextran (or albumin) intravenously.
2. Set the microscope to collect line scans. Obtain a series of line scans (oriented parallel to the vessel walls) in the center of the lumen of several vessels of interest (Fig. 3), collected over a period of several seconds each.

   For simple velocity measures, it is critical to choose for comparison vessels that are of equal diameter.

Data analysis

Analyze line-scan data to determine flow as previously described (Kleinfeld et al., 1998; Ogasawara et al., 2000; Brown et al., 2001; Yamamoto et al., 2002; Kang et al., 2006) based upon the measured slope of the RBC tracks in space-time (XT) images.

BASIC PROTOCOL 4 VASCULAR PERMEABILITY

Alteration in vascular permeability has important pathophysiological consequences in conditions such as inflammation and ischemia-reperfusion injury. Multiphoton microscopy provides a relatively noninvasive method to examine permeability of cortical microvasculature in the kidney (Sutton, Mang et al. 2003, Sutton, Kelly et al. 2005, McCurley, Alimperti et al. 2017).

Materials (per Support Protocol)

Animal

Fluorescent 500,000-Da dextran

Fluorescent 10,000-Da dextran, 40,000-Da dextran, 70,000-Da dextran, 150,000-Da dextran, or fluorescent-labeled bovine serum albumin (choice of probe will depend upon the intrinsic permeability of the vessel of interest)

Isotonic saline, sterile

Additional reagents and equipment for animal preparation

Experimental preparations (per Support Protocol)

1. Surgically prepare the animal.
2. Aliquot fluorescent 500,000-Da dextran (for a dose of 2 mg/kg).
3. Prepare fluorescent-labeled small molecular weight dextran (dose of 15–30 mg/kg in an appropriate volume of sterile, isotonic saline, 0.01–0.03 ml for mice and 0.1–0.2 ml for rats) intravenously.
4. Prepare the microscope. Set laser illumination to 800 nm. Based upon settings determined in similar previous studies, adjust the laser power and detectors such that anticipated maximum signals in the two channels are below saturation. Set detector offset such that a slightly positive signal is obtained from an empty field.

Experimental approach

1. Inject fluorescent 500,000-Da dextran solution intravenously.

   This probe will be used to define the vascular space.
2. Determine the vessel of interest for permeability study and obtain a “pre” image (512-by-128 frame).
3. Rapidly inject fluorescent-labeled small molecular weight dextran solution intravenously.
4. Simultaneous with the dextran injection, begin obtaining a rapid time-series collection (1 to 2 frames/second) of the vessel of interest (Fig. 4).

   It is very useful to optimize the amount and size of the fluorescent probe to be injected in a set of preliminary experiments on the individual setup to be used. The goal is to deliver sufficient probe to the vessel of interest such that the amount leaked from the vessel results in a rapidly detected signal that can be measured, but does not result in saturation of signal levels in the vascular space.

Data analysis

Vessel permeability can be measured utilizing a method previously described by Brown et al. (2001), in which the fluorescence level along a line perpendicular to the vessel is measured as a function of time or by a ratiometric method comparing the change in fluorescent intensity of a region outside the vessel to the change in fluorescent intensity of an adjacent region in the lumen of the vessel over time as described by Yu et al. (2005). Alternatively, if the permeability defect is large enough that larger molecular-weight probes get trapped in the perivascular space, then images of multiple vascular fields can be collected during the experiment and a digital grid can be placed over the image. Permeability can be measured by determining the number of grid segments demonstrating leakage of the fluorescent probe (Sutton et al., 2003).

BASIC PROTOCOL 5 MITOCHONDRIAL FUNCTION

A number of fluorescent probes, such as rhodamine B hexyl ester, accumulate in compartments on the basis of membrane potential. These probes, commonly used to label mitochondria in studies of cultured cells, can also be utilized for intravital fluorescence studies. Whereas mitochondrial probes invariably produce identical staining patterns in cultured cells, their distribution varies widely between different cell types *in vivo* following intravenous introduction. Rhodamine 123 is a green-fluorescing mitochondrial probe that preferentially labels proximal tubule cells (Figure 5B). Tetramethylrhodamine methyl ester, perchlorate (TMRM) is a red-fluorescing dye that labels distal tubules uniformly, and the principal cells of collecting ducts, producing a checkerboard pattern as there is no uptake within the intercalated cells (Figure 5C). (Note that when used at higher concentrations, or with continuous perfusion, TMRM has also been found to label mitochondria in proximal tubule cells in rats and mice (Kalakeche et al., 2011, Hall et al., 2013). Finally Rhodamine B hexyl ester, perchlorate (R6), a red-fluorescing dye labels endothelial cells lining the inner lumen of the peritubular vasculature and glomerular capillary loops, circulating white blood cells, and podocytes which surround the capillary loops (Figure 5A). Below, we describe the use of rhodamine B hexyl ester is used to assay mitochondrial function in the kidney of rats.

Materials (per Support Protocol)

Animal

Rhodamine B hexyl ester

Isotonic saline, sterile

Hoechst 33342 to label nuclei (optional)

Additional reagents and equipment for animal preparation

Experimental preparations (per Support Protocol)

1. Surgically prepare the animal.
2. Prepare 1 ml of a 5 μg/ml working concentration of rhodamine B hexyl ester in sterile, isotonic saline.

   For a standard 200- to 250-g rat, this should be enough for 5 to 8 doses or more (at a dose of 5 μg/kg). This dose will achieve a target dilution in the plasma (not total blood volume) approximately equal to that used in cell culture, 0.1 μg/ml.
3. Aliquot Hoechst 33342 solution (for a dose of 1 mg/kg in 0.5-ml of sterile, isotonic saline).
4. Prepare the microscope. Set laser illumination to 800 nm. Based upon settings determined in similar previous studies, adjust the laser power and detectors such that anticipated maximum signals are below saturation. Set detector offset such that a slightly positive signal is obtained from an empty field.

Experimental approach

1. Infuse Hoechst solution to label nuclei and wait ~5 to 10 min for complete incorporation.
2. While viewing an area through the eyepiece, infuse in the rhodamine B hexyl ester solution.

   An immediate flush of red fluorescence will be visible followed by incorporation into the endothelia and circulating white cells over a period of ~20 to 30 sec.
3. Collect volumes of multiple fields.

Data analysis

Mitochondrial function can be assessed in analyses of single images, or projected image volumes, as the fraction of cells of each type that are positive for the mitochondrial probe. Studies of conditions that might be anticipated to affect microvascular perfusion should be interpreted cautiously since the mitochondrial distribution of probes may reflect not only mitochondrial membrane potential, but also delivery of the probe to a particular cell. In these cases, a large-molecular weight fluorescent dextran may be introduced into the microvasculature to distinguish the effect of perfusion.

BASIC PROTOCOL 6 APOPTOSIS

Apoptosis is a fundamental process in tissue development and injury. The nuclei of all the cells of the kidney can be easily labeled and imaged intravitally, using blue-fluorescing DNA-binding Hoechst 33342 injected intravenously to label nuclei. Nuclear morphology can be reliably used to evaluate apoptosis *in vivo* (Kelly et al., 2003; see Fig. 6). In addition, Hoechst 33342 can be combined with propidium iodide, a red-fluorescing DNA-binding probe, to assay apoptosis and necrosis simultaneously (Dunn et al., 2002). Unlike Hoechst 33342, which is membrane permeant, propidium iodide is membrane impermeant and so labels only nuclei of cells whose plasma membrane is disrupted, as during necrosis.

Materials (per Support Protocol)

Animal

Hoechst 33342

Propidium iodide

Isotonic saline, sterile

Additional reagents and equipment for preparing the animal (Support Protocol)

Experimental preparations (per Support Protocol)

1. Surgically prepare the animal.
2. Prepare Hoechst 33342 and propidium iodide solution. Target doses of 1 mg/kg and 50 μg/kg, respectively, combined in 0.5 ml sterile, isotonic saline.

3. Prepare the microscope. Set laser illumination to 800 nm. Based upon settings determined in similar previous studies, adjust the laser power and detectors such that anticipated maximum signals are below saturation. Set detector offset such that a slightly positive signal is obtained from an empty field.

Experimental approach

1. Collect images in blue, red, and green channels.

   These images will serve as “background” images.

2. Inject Hoechst 33342/propidium iodide solution intravenously.

3. After ~15 min, find suitable fields for imaging. Ensure that the animal and the field are stable and collect images in red, green, and blue channels.

Data analysis

Visually score the fraction of cells that are apoptotic and/or necrotic. Insofar as unbound propidium iodide is rapidly cleared from the circulation, propidium iodide should be repeatedly introduced for studies evaluating changes in the incidence of necrosis over time. Healthy cells are characterized by nuclear labeling by Hoechst, but not propidium iodide, with an intact, regular nuclear morphology. Primary apoptotic cells are characterized by a fragmented nuclear labeling with Hoechst, but not propidium iodide. Necrotic cells are characterized by nuclear labeling with both Hoechst and PI, and an intact, regular nuclear morphology. Apoptotic cells with secondary necrosis are characterized by nuclear labeling with both Hoechst and PI, and a fragmented nuclear morphology. Thus rates of apoptosis, necrosis, and apoptosis with secondary necrosis can be scored as the fraction of cells per field observed, and categorized by cell type, tubular segment, and so on.

SUPPORT PROTOCOL ANESTHESIA AND SURGICAL CREATION OF A RETROPERITONEAL SURGICAL WINDOW FOR INTRAVITAL IMAGING

The surgical procedure described is for a non-survival surgery in which image acquisition is the final step before the animal is sacrificed. Appropriate steps need to be taken to insure rigorous sterile technique if animal survival following image acquisition is planned (for example for longitudinal studies of the same animal). The retroperitoneal surgical window is designed for imaging using a microscope in an inverted configuration, which we have found is preferred for intravital microscopy of the rodent kidney (see discussion in the “Special Equipment” section)

Materials

Animal to be imaged

5% (v/v) and 2% (v/v) isoflurane/oxygen mixtures

Pentabarbital (optional)

Buprinorphine

Germicidal soap

0.9% sterile saline, prewarmed

Appropriate probes

Anesthesia induction chamber (Braintree Scientific)

Homeothermic table (Braintree Scientific)

Rectal probe (Braintree Scientific)

Electric clippers

Vascular catheters (PE-60 tubing for rats and PE-50 tubing for mice; Becton Dickinson) Kidney cup

Surgical scissors (Braintree Scientific)

Appropriate temperature control devices (e.g., circulating water blanket attached to a temperature-controlled circulating water bath, Repti Therm heating pad)

Prepare animal for surgery

1 Place the animal to be imaged into an anesthesia induction chamber containing a 5% isoflurane/oxygen mixture.

General anesthesia with intravenous anesthetic agents is an alternative approach.

2 After initial anesthesia is obtained, rapidly move the animal from the induction chamber to a clean surgical area on a homeothermic table. Maintain anesthesia with a 2% isoflurane/oxygen mixture titrated to effect.

3 Inject 0.05 mg/kg buprinorphine subcutaneously.

4 Shave the left flank area and any areas requiring vascular catheter insertion (i.e., neck for internal jugular, inner thigh for femoral) using electric clippers. Cleanse the respective areas with germicidal soap and water and then towel dry.

5 Insert rectal probe for temperature monitoring.

Perform surgery

6 Make a small incision (using surgical scissors) over the desired vessels to be accessed and insert the appropriate vascular catheters (PE-60 tubing for rats and PE-50 tubing for mice).

7 Make a 0.5- to 1-cm incision (using surgical scissors) in the left flank through the retroperitoneum to expose the left kidney.

8 Move the animal to the microscope stage and position the left kidney covered with prewarmed saline next to the objective while maintaining appropriate anesthesia.

Lay the animal over the objective with the kidney in contact with the objective (Fig. 7).

9 Employ appropriate temperature control devices.

This can be accomplished by covering the animal in a circulating water blanket attached to a temperature-controlled circulating water bath and two Repti Therm heating pads placed beneath the rat (one below the head and one below the thighs as close to the coverslip dish as possible to maximize contact with the rat;

10 Introduce appropriate probes via intravenous injection, making sure to flush dead space of catheter.

11 Monitor depth of anesthesia, core body temperature, and blood pressure (if desired) during image acquisition.

REAGENTS AND SOLUTIONS

Use deionized, distilled water in all recipes and protocol steps. For common stock solutions, see APPENDIX 2A; for suppliers, see SUPPLIERS APPENDIX.

Hoechst 33342

10 mg/ml in sterile distilled water (Invitrogen)

Bovine serum albumin (conjugated to fluorescent label of choice; see Dextrans recipe for fluorescent conjugates)

10 mg/ml in 0.9% sterile saline.

Store fluorophore-conjugated albumin wrapped in foil ≤1 month at 4°C.

Dextrans (3,000-, 10,000- 40,000-, 70,000-, and 500,000-Da dextrans conjugated to fluorescent label of choice)

3,000, 10,000, 40,000, 70,000-Da, and 150,000-Da fluorescently conjugated (see below) dextrans: 20 mg/ml in 0.9% sterile saline.

500,000-Da fluorescently conjugated (see below) dextran: 8 mg/ml in 0.9% (w/v) sterile saline, dialyze 5 to 10 ml using a 10,000 MWCO membrane against 0.9% (w/v) sterile saline (5 liters) overnight at room temperature.

Store all fluorophore-conjugated dextrans wrapped in foil ≤1 month at 4°C.

Fluorescent conjugates—Fluorescent conjugates may be either purchased directly, or prepared using reactive fluors. The choice of fluor to use for multiphoton microscopy is never obvious. Very few organic probes have been characterized for multiphoton microscopy, and the simple rule of doubling the one-photon excitation wavelength for two-photon excitation is seldom effective The reader is referred to published two photon action cross sections (Xu et al., 1996, Kobat et al., 2009, Mutze et al., 2012) and to data posted

online by Warren Zipfel's laboratory (http://www.drbio.cornell.edu/cross_sections.html). The authors have obtained excellent results using fluorescent conjugates prepared with fluorescein, rhodamine, Texas Red, and Cascade Blue using excitation wavelengths centered around 800 nm.

Rhodamine B hexyl ester

5 mg/ml rhodamine B hexyl ester in dimethylformamide (DMF), anhydrous (store wrapped in foil ≤6 months at—20°C)

Propidium iodide

5 mg/ml propidium iodide in sterile water.

COMMENTARY

Background Information

Intravital microscopy is a powerful research technique that brings the speed, temporal resolution, and multiparameter capabilities of microscopy to the study of intact, living organisms. Thus, powerful microscopy approaches previously limited to studies of cultured cells may be applied to study of cell biology in physiological, differentiated cells in the relevant context of the living organism, with all systemic interactions intact.

Intravital microscopy has been applied to studies of the kidney for over 100 years. In part this reflects the ease with which the kidney can be presented to the microscope objective lens, combined with the wealth of microvascular and tubular processes that can be easily imaged at the surface of the cortical surface of the kidney. Microscopic analysis of kidney function *in vivo* is also facilitated by the fact that many of the functions of the kidney are easily evaluated using probes introduced intravenously, or into tubule lumens via micropuncture. An excellent review of the use of intravital microscopy for studies of kidney function is found in Steinhausen and Tanner (1976).

Intravital microscopy is enjoying a renaissance, thanks to the development of multiphoton microscopy (Denk et al., 1990; Denk and Svoboda, 1997; Zipfel et al., 2003; Dunn and Young, 2006). This technique, which depends upon the simultaneous absorption of two infrared photons by a fluorophore, resulting in spatially localized fluorescence excitation, is capable of collecting high-resolution (0.4 μm) fluorescence images deep into tissues (Centonze and White, 1998). In addition to providing better penetration and resolution than traditional methods of microscopy, the use of infrared light also makes multiphoton microscopy significantly less toxic to living systems (Squirrell et al., 1999). Thus multiphoton has been used to extend the reach of intravital fluorescence microscopy hundreds of microns into the tissues of intact, living animals, with minimal damage.

In some of its earliest applications, itravital multiphoton microscopy was applied to analyze skin structure (Masters et al., 1997), angiogenesis, blood-flow and tumor-cell dynamics in skinfold preparations (Brown et al., 2001; Condeelis and Segall, 2003), and blood flow, neural development, and neural activity in the superficial layers of the brain (Denk and Svoboda, 1997; Svoboda et al., 1997; Kleinfeld et al., 1998; Helmchen et al., 1999). Over

the past twenty years, intravital multiphoton microscopy has has been combined with surgical procedures to support imaging of internal organs, applications in which it has been used to study a wide range of physiological and pathophysiological processes at subcellular resolution *in vivo* (Cahalan and Parker, 2006, Weigert et al., 2010, Ellenbroek et al., 2014, Okada et al., 2016, Schiessel et al., 2016).

With respect to the kidney, investigators in the nephrology community have increasingly utilized intravital multiphoton microscopy to examine a wide variety of parameters under both physiological and pathophysiological conditions. Intravital microscopy has provided important insights into podocyte biology, glomerular function, and tubular handling of albumin (Russo, Sandoval et al. 2007, Yu, Sandoval et al. 2007, Nakano, Kobori et al. 2012, Hackl, Burford et al. 2013, Schiessl and Castrop 2013, Burford, Villanueva et al. 2014, Ferrell, Sandoval et al. 2015, Schiessl, Kattler et al. 2015, Brahler, Yu et al. 2016, Schiessl, Hammer et al. 2016, Wagner, Campos-Bilderback et al. 2016). Intravital microscopy has been applied to study proximal tubule transport (Tanner et al., 2004), organic cation uptake (Horbelt, Wotzlaw et al. 2007), and folate uptake (Sandoval et al., 2004) in the proximal tubule as well as tubular metabolism (Hato, Friedman et al. 2016, Hato, Winfree et al. 2017). In addition, intravital microscopy has been employed to advance our understanding of the tubular, microvascular, and immunologic alterations during ischemic and septic acute kidney injury (AKI) at regional (sub-organ), cellular, and sub-cellular resolution (Sutton, Mang et al. 2003, Sutton, Kelly et al. 2005, Gupta, Rhodes et al. 2007, Sharfuddin, Sandoval et al. 2009, Imamura, Isaka et al. 2010, Basile, Friedrich et al. 2011, Kalakeche, Hato et al. 2011, Hall, Rhodes et al. 2013, Hato, Sandoval et al. 2015, Nakano, Doi et al. 2015, McCurley, Alimperti et al. 2017). Intravital microscopy has also been helpful in elucidating alterations in the transplanted kidney (Camirand, Li et al. 2011) and in the kidney during systemic and local infection (Choong, Regberg et al. 2012, Yatim, Gosto et al. 2016). Selected overviews of the use of intravital multiphoton microscopy for studies of renal function can be found in Dunn et al. (Dunn, Sandoval et al. 2002), Peti-Peterdi et al. (Peti-Peterdi, Burford et al. 2012), and Hall and Molitoris (Hall and Molitoris 2014).

Special equipment

Microscope system: While intravital microscopy of the kidney can be conducted with nearly any kind of epi-illumination microscope system, the need for optical sections favors either confocal or multiphoton microscopy. Multiphoton microscopy has several advantages over confocal microscopy, supporting deeper imaging into scattering tissues (Centonze and White, 1998; Konig, 2000) with minimal adverse physiological and photophysical effects (Squirrell et al., 1999). Once the province of specialized laboratories, multiphoton microscope systems are now commercially available from a number of companies. Alternatively, numerous investigators have successfully built their own systems, allowing them to customize the system according to their specific needs (Majewska et al., 2000; Nguyen et al., 2001; Muller et al., 2003). In many cases, multiphoton microscope systems can be adapted from existing confocal microscope systems with relatively minor modifications. When purchasing or modifying a system, it is critical that the optical lightpath is compatible with the IR illumination wavelengths that you intend to use, efficiently transmitting illumination to the sample and efficiently blocking illumination from

the detectors. The optics of a system with a titanium-sapphire laser need to efficiently accommodate wavelengths out to around 1000 nm, whereas those using an optical parametric oscillator-based system need to accommodate wavelengths out to around 1300 nm.

Microscope systems can be configured in either an upright design, in which the microscope objective is located above the stage, or an inverted design, in which the microscope objective is located below the stage. While both can be used for intravital imaging of the kidney, we have found the inverted configuration to be far simpler and more reliable. The issue here is that while the kidney is easily presented to an objective lens from above, it is subject to excessive movement, due to respiration. The kidney can be immobilized by placing it in a "kidney cup" inserted into the body of the animal (Figure 7). However, the device is invasive (particularly for mice), proper kidney function depends upon careful placement in order to avoid constricting blood or urine flow and its effectiveness varies according to how closely the kidney fits into the cup. As will be described in a later section, intravital microscopy of the rodent liver can be easily accomplished using an inverted microscope configuration by simply laying the exteriorized kidney onto a glass coverslip-bottomed dish placed on the microscope stage. The weight of the animal serves to minimize or eliminate respiration induced motion in the kidney.

Multiphoton excitation fluorescence microscopy is based upon collecting an image generated by scanning a laser over a sample. The scanning mechanism can be based upon a galvanometer, which will support imaging of reasonably -sized fields at a rate of 1–3 frames per second or can be based upon a resonant-scanner, which will support imaging at rates over 30 frames per second. However, realizing this kind of speed depends upon samples with sufficient fluorescence to provide usable signals despite a 10–30 fold shorter pixel dwell time. In our studies of the kidney, we have found very few applications that provide fluorescence sufficient to capitalize on the additional speed provided by a resonant scanning system.

Alternatively, the speed of image capture can be increased by splitting laser illumination into multiple beamlets that are simultaneously scanned over the sample. Fluorescence emissions are then collected on a 2D field detector, such as a charge-coupled device (CCD). In principle, the rate of image capture can be increased in direct proportion to the number of beamlets, limited only by the available laser power. In studies of brain slices, a "multifocal" two-photon microscope system was capable of increasing the speed of image capture 60-fold (Niesner et al., 2007). These kinds of speeds are unlikely to be reached in highly scattering tissues such as the kidney, which require significant power to accomplish penetration of even a single beam into the tissue. Insofar as scattered emissions are imaged as a diffuse background on the field detector, scattering will also compromise the signal-to-background ratio of images collected at depth by a multifocal system. Finally, the use of a field detector compromises the ability to collect multiplexed fluorescence data. Whereas single-point scanning systems support simultaneous imaging of 3 or 4 different fluorophores, the use of a field detector generally requires sequential imaging of individual fluorophores.

In our experience, the potential benefits of resonant scanning and multifocal scanning systems are rarely useful for intravital microscopy of the rodent kidney, and so our work has almost exclusively been conducted using galvanometer-based single point scanning systems. The frame rate provided by these systems is typically high enough to capture moderately fast dynamic events such as glomerular filtration, but not fast enough to capture processes such as blood flow or vascular leakage. For these faster processes, the rate of image capture can be increased by limiting the number of lines scanned (scanning a smaller region). Frame rate increases almost linearly as the number of scanned lines decreases. At the limit, one may collect an “image” of a single line in the sample. These “line scan” images can be captured at a rate of more than 480 lines per second. As described in a previous section, this approach can be used to capture the dynamics of a process traversing along the axis of the line scan, such as blood flow or vascular leakage.

Microscope objective lens: Multiphoton microscopy of the kidney places unique requirements on the microscope objective lens. First, the objective should efficiently transmit the range of excitation wavelengths provided by the laser system. Second, the objective should be designed with a working distance sufficient to reach the cells of interest.

Third, the objective lens should be designed with a largenumerical aperture (NA) A large NA is preferred not only for resolution, but also for efficient multiphoton excitation of fluorescence. The issue of NA is complicated however, since high-NA objectives show a steep attenuation of signal with depth, owing to the loss of peripheral rays to scattering and to theirgreater susceptibility to spherical aberration, as results from refractive index mismatch. The refractive index of the kidney has been estimated at ~1.4, which is intermediate between that of water and glass. Accordingly, the refractive index of the immersion medium differs from that of the kidney with either water- or oil-immersion objectives. In both cases, this mismatch results in spherical aberration that increases with depth, significantly reducing multiphoton excitation. Despite this, both oil- and water-immersion objectives have been used to collect images up to 150 μm into the kidney of living animals (Dunn et al., 2002; Kelly et al., 2003; Sutton et al., 2003; Sandoval et al., 2004; Tanner et al., 2004; Molitoris and Sandoval, 2005; Sutton et al., 2005; Yu et al., 2005; Kang et al., 2006; Rosivall et al., 2006; Toma et al., 2006; Russo et al., 2007). Recently developed objectives have addressed the challenge of spherical aberration in high NA objectives by designing them for use with immersion media whose refactive index better matches that of the kidney, for example silicone oil (refractive index 1.40) or glycerol (refractive index 1.45). A glycerol immersion objective was used in studies of glomerular permeability in rats and mice (Nakano et al., 2012).

Finally, the objective lens may be designed for use with a coverslip, or in the case of “dipping objectives,” designed for use without a coverslip. Imaging with an inverted microscope obviously requires the use of a coverslip. While dipping objectives can be used with upright microscopes, the authors have found that the normal curvature of the kidney is such that it limits the region that can be imaged to a small region at the apex of the exposed kidney. A much larger region of the kidney may be imaged when its surface is gently depressed with a coverslip.

Laser system: Multiphoton microscopy requires a specialized laser capable of providing very powerful, very brief pulses of IR light. Most systems employ titanium-sapphire lasers, which are tunable across a wavelength range from around 700 to 1050 nm. These systems typically provide highest power at intermediate wavelengths, but are nonetheless useful in that they can be tuned to optimize particular fluors. A simpler alternative is the neodymium laser, which provides a single 1047-nm excitation wavelength. Titanium-sapphire lasers may be configured to provide pulses of picosecond duration (picosecond lasers), and of 100- to 300-fsec durations. While picosecond lasers are capable of multiphoton excitation, femtosecond lasers are generally preferred, owing to the fact that they stimulate more fluorescence for the same average power delivered to the tissue.

Recently, new laser systems have become commercially available that extend illuminations out to 1300 nm, and microscope manufacturers have responded by modifying their optics for compatibility with these extended wavelengths. Insofar as these systems are better suited to excitation of fluorescent probes and proteins that emit in the orange-to-red spectrum, they may support imaging into deeper reaches of biological tissues. In many cases, these sytems also provide the ability to illuminate samples with two IR beams at once, extending the capacity for multiplexed imaging.

While it may be argued that power is not limiting in multiphoton microscopy and that the laser systems provide many times more power than is necessary to saturate fluorophores, laser power can become limiting at depth in tissues. Owing to scattering, absorption, and spherical aberration, much of the illuminating light fails to reach the focus at depth in tissue. For this reason, the authors frequently find that stimulation of satisfactory levels of fluorescence at depth requires the delivery of >50 mW at the surface of the kidney. Given the 80% to 90% losses of illumination in the optical system, it is thus important to obtain a laser system providing at least 700 mW of power (at a wavelength of 800 nm).

Multiphoton laser systems are actually simpler than confocal microscopes but until recently their use was complicated by the fussy laser systems. In the past 15 years, this problem has essentially disappeared with the development of “closed-box,” computer-controlled laser systems that seldom require attention from the user. In addition to supporting automated adjustment of illumination wavelength, these systems also automatically adjust beam alignment, beam diameter and dispersion compensation.

Fluorescence detection systems: Because fluorescence excitation is spatially constrained in multiphoton fluorescence microscopy, fluorescence emissions must be collected only rather than imaged. Thus, large-area detectors may be used to collect both ballistic and scattered emissions. The efficiency of collection of scattered photons is increased as the distance to the detector is reduced, and thus the most efficient systems are designed with “nondescanned” detectors located as close as possible to the plane of the back aperture of the objective lens. In modified confocal microscope systems, it is also possible to collect emissions via the same descanned detectors used for confocal microscopy. However, these systems sacrifice sensitivity in the inevitable losses of light in the descanning optics, and the losses of scattered light in the elongated lightpath.

Light collection may be split among multiple photomultiplier tubes, so that multiple colors of fluorescence may be imaged simultaneously. Although these systems suffer from significant between-channel crosstalk, owing to the simultaneous excitation of multiple fluors, they are invaluable to intravital microscopy. Such systems support ratiometric measurements, comparisons of multiple parameters, and independent labeling of structures for identification and processes for functional analysis, and also facilitate identification of tissue autofluorescence, which has a characteristic, multichannel spectral signature. While most systems can be equipped with detectors on both the epi- and trans-illumination sides of the sample, only detectors on the epi-illumination pathway will be capable of collecting fluorescence from the kidney of a living animal.

Whereas early systems utilized conventional multi-alkali photomultiplier tube detectors, all commercial vendors now offer systems utilizing more sensitive (and expensive) detectors, such as gallium arsenide phosphide (GaAsP) detectors, or hybrid GaAsP detectors. These new designs offer significant advantages for high-speed or photon-limited imaging, but can also be challenging to use as they can be damaged by high photon fluxes, and so include circuitry to shut themselves down upon detection of excessive signal.

Adaptations of the microscope stage for imaging living animals: The primary considerations for imaging living animals pertain to presenting the tissue within the narrow range of the microscope objective, immobilizing the tissue, and maintaining the tissue and the animal itself at physiological temperature. The stage of most microscopes is typically large enough to support rats and mice. Special stages and alternative microscope designs must be used for larger animals.

The exteriorized kidney is placed into a 50-mm-diameter cell-culture dish whose bottom has been fitted with a number 1 1/2 cover slip (Warner Instruments), filled with saline (Figure 8). The specifics of each of these methods are presented below. Anesthetized animals require auxiliary sources of heat to maintain their body temperature. The authors typically accomplish this by topically warming the animal with a heated water jacket (TPZ-1215VF on a TPZ-747 Micro-Temp LT circulation pump, Kent Scientific, Torrington) and heating the stage with a surface heater (an aluminum plate fitted with two Kapton heat mats (Cole-Parmer) controlled with a custom-built TET-612 temperature controller, and a T-type thermistor probe. When using immersion objectives, it is critical to heat the objective lens, which can otherwise act as a local heat sink, thus cooling the tissue in proximity to the objective lens. The authors are currently using OW series objective warmers along with TC124 controllers (Warner Instruments). Alternatively, the entire microscope stage may be enclosed in a heated chamber. This second alternative heats both the animal and the objective lens, and provides excellent temperature control, but complicates access to the animal during the course of imaging.

Equipment for preparing and maintaining animals: Generally, the standard surgical equipment utilized in small animal surgery is sufficient for preparing rodents for intravital microscopy. PE-50 or PE-60 hollow tubing is a useful size for intravenous (internal jugular, femoral) and intra-arterial (femoral) catheters placed for probe delivery and animal monitoring. A calibrated anesthetic vaporizer and a closed anesthesia circuit with a rubber

diaphragm that fits snugly over the snout of the animal is required if inhaled anesthetics are to be used. A charcoal canister attached to the exhalation vent of the anesthesia circuit is necessary for scavenging volatile anesthetic waste. Requisite equipment to adapt the microscope stage for intravital imaging is discussed in the preceding section.

Once the animal is appropriately positioned on the stage, monitoring the animal's depth of anesthesia, core temperature, and blood pressure during imaging are important considerations. The depth of anesthesia can be sufficiently monitored by visual inspection of respiration rate, peripheral perfusion, and the lack of withdrawal reflexes following tail or leg pinch. A rectal temperature probe coupled to a thermometer is a customary method to monitor the animal's core temperature. Blood pressure can be monitored with a transducer/amplifier system attached to a femoral artery catheter or by commercially available noninvasive blood-pressure monitoring devices.

Equipment for digital image analysis: When combined with digital image analysis, multiphoton microscopy is capable of being a truly quantitative tool. Since image analysis is a time-consuming task, it is generally most expedient to perform image analysis on a separate computer system dedicated to image analysis, rather than conducting image analysis on the computer associated with the microscope system. Owing to the recent development of inexpensive, powerful personal computer systems, it is not difficult to find a computer system capable of conducting most forms of image analysis. That said, multiphoton microscopy is capable of generating enormous datasets–image volumes consisting of 200 image planes in three channels are not uncommon and when digitized to 12 bits occupy more than 300 Mb of memory. The memory requirements increase for many forms of image analysis in which multiple copies of an image volume may need to be stored and for studies conducted in time series. In a world where typical operating systems require >100 Mb of memory, it is clear that users should configure systems with as much memory as their systems will accommodate. Image-analysis systems thus also need to be configured with sufficient storage for large numbers of such data sets, as well as a system for archiving data to digital video disk or some alternative.

Suitable image-analysis software is available for purchase commercially, or via shareware. For routine, quantitative analysis the authors' group favors the commercial Metamorph image-analysis software and the ImageJ freeware. For volumetric analysis, the group utilizes the commercially available Imaris software, and Voxx visualization and VTEA image analysis software, which was developed in-house (Clendenon, Phillips et al. 2002, Winfree, Khan et al. 2017).

Critical Parameters and Troubleshooting

Animal support considerations and problems—Alterations of core temperature and blood pressure can have a significant impact upon the processes examined by the protocols outlined in this unit. Consequently, monitoring and controlling these two parameters throughout the image acquisition process as previously outlined is essential.

Stability of the sample—The ability of multiphoton microscopy to provide sub-micron resolution depends critically upon minimizing the effects of even the most subtle body

movements. In large part, this can be accomplished by ensuring adequate anesthesia. However, significant movement of the microscopic field can result from respiration and the heartbeat. These factors can be minimized through optimizing the plane of anesthesia. As a last resort, adhering the kidney to the coverslip via a cyanoacrylate adhesive can aid in further diminishing motion artifact.

Effects of injection of probes—In general, the probes utilized in these protocols are inert and have minimal interaction with other homeostatic mechanisms in the animal. The probes can be rapidly injected (over the course of seconds) in small volumes to rodents (<100 to 200 μl; max 5mL/kg) without significant alterations in animal stability.

Fluorescence bleedthrough—Owing to the need for high-speed image capture and to the fact that changing excitation wavelengths is a relatively slow process with current laser technology, most multi-parameter studies involve the simultaneous collection of the fluorescence of multiple fluors excited by a single excitation wavelength. This approach almost inevitably leads to “bleed-through” of fluorescent signals between channels, typically where a fraction of the emissions of one fluor is collected in the channel intended to collect those of a fluor emitting at a longer wavelength. To some extent, this problem can be minimized though the use of probes whose fluorescence distributions are known to be distinct from one another. So, for example, while the blue fluorescence of Hoechst bleeds into the channel collecting the green fluorescence of a fluorescein dextran in the vasculature, no bleedthrough will be found in the image of the vascular lumen, and the appearance of nuclear fluorescence in the green detector channel is not confusing. When it is not possible to design studies in which the distribution of spectrally adjacent signals are distinct, researchers can minimize crosstalk by using short wavelength–emitting fluors for the probe with a weaker signal, and longer wavelength–emitting fluors for the probe with a stronger signal. To some degree, the relative fluorescence of different fluors can be adjusted by shifting the excitation wavelength one direction or the other.

Tissue autofluorescence—Careful choice of fluorescent probes and excitation wavelength can also minimize the consequences of endogenous autofluorescence. So, for example, the authors find that the endogenous autofluorescence of lysosomes of proximal kidney cells can be minimized by shifting the excitation wavelength from 800 to 860 nm. To the degree that such manipulations are not possible, autofluorescence may also be identified by its characteristic spectral signature. The authors find that lysosomal autofluorescence can be identified by its broad spectrum throughout the green-to-red range, when excited at 800 nm.

Anticipated Results

Intravital multiphoton microscopy can be expected to provide high-resolution imaging deep into the kidney of a living rodent with frame rates on the order of one per second. As described above, these studies can yield unique, quantitative evaluations of numerous renal functions. In addition, because of the unique view of renal function provided by this technique, investigators frequently observe unforeseen phenomena beyond those anticipated in the original study design.

Time Considerations

Preparation of the animal for imaging depends upon the technical expertise of the operator. A reasonable estimate of the time from induction of anesthesia to the first image collected is ~30 min depending on the experiment. Time estimates for image collection depend upon the particular experiment, but animals can be adequately maintained on the microscope stage for 3 hr or more.

Acknowledgments

This research was supported by NIH-NIDDK P30 DK079312, Center for Advanced Renal Microscopic Analysis awarded to Kenneth Dunn. All studies were conducted at the Indiana Center for Biological Microscopy.

Literature Cited

Basile DP, Friedrich JL, Spahic J, Knipe N, Mang H, Leonard EC, Changizi-Ashtiyani S, Bacallao RL, Molitoris BA, Sutton TA. Impaired endothelial proliferation and mesenchymal transition contribute to vascular rarefaction following acute kidney injury. Am J Physiol Renal Physiol. 2011; 300(3):F721–733. [PubMed: 21123492]

Brahler S, Yu H, Suleiman H, Krishnan GM, Saunders BT, Kopp JB, Miner JH, Zinselmeyer BH, Shaw AS. Intravital and Kidney Slice Imaging of Podocyte Membrane Dynamics. J Am Soc Nephrol. 2016; 27:3285–90. [PubMed: 27036737]

Brown EB, Campbell RB, Tsuzuki Y, Xu L, Carmeliet P, Fukumura D, Jain RK. *In vivo* measurement of gene expression, angiogenesis and physiological function in tumors using multiphoton laser scanning microscopy. Nat Med. 2001; 7:864–868. [PubMed: 11433354]

Burford JL, Villanueva K, Lam L, Riquier-Brison A, Hackl MJ, Pippin J, Shankland SJ, Peti-Peterdi J. Intravital imaging of podocyte calcium in glomerular injury and disease. J Clin Invest. 2014; 124(5): 2050–2058. [PubMed: 24713653]

Cahalan MD, Parker I. Imaging the choreography of lymphocyte trafficking and the immune response. Curr Opin Immunol. 2006; 18:476–482. [PubMed: 16765574]

Camirand G, Li Q, Demetris AJ, Watkins SC, Shlomchik WD, Rothstein DM, Lakkis FG. Multiphoton intravital microscopy of the transplanted mouse kidney. Am J Transplant. 2011; 11:2067–74. [PubMed: 21834913]

Centonze VE, White JG. Multiphoton excitation provides optical sections from deeper within scattering specimens than confocal imaging. Biophys J. 1998; 75:2015–2024. [PubMed: 9746543]

Choong FX, Regberg J, Udekwu KI, Richter-Dahlfors A. Intravital models of infection lay the foundation for tissue microbiology. Future Microbiol. 2012; 7(4):519–533. [PubMed: 22439728]

Clendenon JL, Phillips CL, Sandoval RM, Fang S, Dunn KW. Voxx: a PC-based, near real-time volume rendering system for biological microscopy. Am J Physiol Cell Physiol. 2002; 282(1):C213–218. [PubMed: 11742814]

Condeelis J, Segall JE. Intravital imaging of cell movement in tumours. Nat Rev Cancer. 2003; 3:921–930. [PubMed: 14737122]

Denk W, Svoboda K. Photon upmanship: Why multiphoton imaging is more than a gimmick. Neuron. 1997; 18:351–357. [PubMed: 9115730]

Denk W, Strickler JH, Webb WW. Two-photon laser scanning fluorescence microscopy. Science. 1990; 248:73–76. [PubMed: 2321027]

Dunn KW, Young PA. Principles of multiphoton microscopy. Nephron Exp Nephrol. 2006; 103:e33–e40. [PubMed: 16543762]

Dunn KW, Sandoval RM, Kelly KJ, Dagher PC, Tanner GA, Atkinson SJ, Bacallao RL, Molitoris BA. Functional studies of the kidney of living animals using multicolor two-photon microscopy. Am J Physiol Cell Physiol. 2002; 283:C905–C916. [PubMed: 12176747]

Ellenbroek SI, van Rheenen J. Imaging hallmarks of cancer in living mice. Nat Rev Cancer. 2014; 14(6):406–418. [PubMed: 24854083]

Ferrell N, Sandoval RM, Bian A, Campos-Bilderback SB, Molitoris BA, Fissell WH. Shear stress is normalized in glomerular capillaries following (5/6) nephrectomy. Am J Physiol Renal Physiol. 2015; 308:F588–93. [PubMed: 25587117]

Ghiron M. Uber eine neue Methode mikroskopischer Untersuchung em lebenden Organismus. Zbl Physiol. 1912; 26:613–617.

Gupta A, Rhodes GJ, Berg DT, Gerlitz B, Molitoris BA, Grinnell BW. Activated protein C ameliorates LPS-induced acute kidney injury and downregulates renal INOS and angiotensin 2. Am J Physiol Renal Physiol. 2007; 293:F245–54. [PubMed: 17409278]

Hackl MJ, Burford JL, Villanueva K, Lam L, Susztak K, Schermer B, Benzing T, Peti-Peterdi J. Tracking the fate of glomerular epithelial cells *in vivo* using serial multiphoton imaging in new mouse models with fluorescent lineage tags. Nat Med. 2013; 19:1661–6. [PubMed: 24270544]

Hall AM, Molitoris BA. Dynamic multiphoton microscopy: focusing light on acute kidney injury. Physiology (Bethesda). 2014; 29(5):334–342. [PubMed: 25180263]

Hall AM, Rhodes GJ, Sandoval RM, Corridon PR, Molitoris BA. *In vivo* multiphoton imaging of mitochondrial structure and function during acute kidney injury. Kidney Int. 2013; 83:72–83. [PubMed: 22992467]

Hato T, Friedman AN, Mang H, Plotkin Z, Dube S, Hutchins GD, Territo PR, McCarthy BP, Riley AA, Pichumani K, Malloy CR, Harris RA, Dagher PC, Sutton TA. Novel application of complementary imaging techniques to examine *in vivo* glucose metabolism in the kidney. Am J Physiol Renal Physiol. 2016; 310:F717–F25. [PubMed: 26764206]

Hato T, Sandoval R, Dagher PC. The caspase 3 sensor Phiphilux G2D2 is activated non-specifically in S1 renal proximal tubules. Intravital. 2015; 4

Hato T, Winfree S, Day R, Sandoval RM, Molitoris BA, Yoder MC, Wiggins RC, Zheng Y, Dunn KW, Dagher PC. Two-Photon Intravital Fluorescence Lifetime Imaging of the Kidney Reveals Cell-Type Specific Metabolic Signatures. J Am Soc Nephrol. 2017

Helmchen F, Svoboda K, Denk W, Tank DW. *In vivo* dendritic calcium dynamics in deep-layer cortical pyramidal neurons. Nat Neurosci. 1999; 2:989–996. [PubMed: 10526338]

Horbelt M, Wotzlaw C, Sutton TA, Molitoris BA, Philipp T, Kribben A, Fandrey F, Pietruck F. Organic cation transport in the rat kidney *in vivo* visualized by time-resolved two-photon microscopy. Kidney Int. 2007; 72:422–9. [PubMed: 17495857]

Imamura R, Isaka Y, Sandoval RM, Ori A, Adamsky S, Feinstein E, Molitoris BA, Takahara S. Intravital two-photon microscopy assessment of renal protection efficacy of siRNA for p53 in experimental rat kidney transplantation models. Cell Transplant. 2010; 19:1659–70. [PubMed: 20719069]

Kalakeche R, Hato T, Rhodes G, Dunn KW, El-Achkar TM, Plotkin Z, Sandoval RM, Dagher PC. Endotoxin uptake by S1 proximal tubular segment causes oxidative stress in the downstream S2 segment. J Am Soc Nephrol. 2011; 22:1505–16. [PubMed: 21784899]

Kang JJ, Toma I, Sipos A, McCulloch F, Peti-Peterdi J. Quantitative imaging of basic functions in renal (patho)physiology. Am J Physiol Renal Physiol. 2006; 291:F495–F502. [PubMed: 16609147]

Kelly KJ, Sandoval RM, Dunn KW, Molitoris BA, Dagher PC. A novel method to determine specificity and sensitivity of the TUNEL reaction in the quantitation of apoptosis. Am J Physiol Cell Physiol. 2003; 284:C1309–C1318. [PubMed: 12676658]

Kleinfeld D, Mitra PP, Helmchen F, Denk W. Fluctuations and stimulus-induced changes in blood flow observed in individual capillaries in layers 2 through 4 of rat neocortex. Proc Natl Acad Sci USA. 1998; 95:15741–15746. [PubMed: 9861040]

Kobat D, Durst ME, Nishimura N, Wong AW, Schaffer CB, Xu C. Deep tissue multiphoton microscopy using longer wavelength excitation. Opt Express. 2009; 17(16):13354–13364. [PubMed: 19654740]

Konig K. Multiphoton microscopy in life sciences. J Microsc. 2000; 200:83–104. [PubMed: 11106949]

Majewska A, Yiu G, Yuste R. A custom-made two-photon microscope and de-convolution system. Pflugers Arch. 2000; 441:398–408. [PubMed: 11211128]

Masters BR, So PT, Gratton E. Multiphoton excitation fluorescence microscopy and spectroscopy of *in vivo* human skin. Biophys J. 1997; 72:2405–2412. [PubMed: 9168018]

McCurley A, Alimperti S, Campos-Bilderback SB, Sandoval RM, Calvino JE, Reynolds TL, Quigley C, Mugford JW, Polacheck WJ, Gomez IG, Dovey J, Marsh G, Huang A, Qian F, Weinreb PH, Dolinski BM, Moore S, Duffield JS, Chen CS, Molitoris BA, Violette SM, Crackower MA. Inhibition of alphavbeta5 Integrin Attenuates Vascular Permeability and Protects against Renal Ischemia-Reperfusion Injury. J Am Soc Nephrol. 2017; 28:1741–1752. [PubMed: 28062569]

Molitoris BA, Sandoval RM. Intravital multiphoton microscopy of dynamic renal processes. Am J Physiol Renal Physiol. 2005; 288:F1084–F1089. [PubMed: 15883167]

Muller M, Schmidt J, Mironov SL, Richter DW. Construction and performance of a custom-built two-photon laser scanning system. J Phys D: Appl Phys. 2003; 36:1747–1757.

Mutze J, Iyer V, Macklin JJ, Colonell J, Karsh B, Petrasek Z, Schwille P, Looger LL, Lavis LD, Harris TD. Excitation spectra and brightness optimization of two-photon excited probes. Biophys J. 2012; 102:934–44. [PubMed: 22385865]

Nakano D, Doi K, Kitamura H, Kuwabara T, Mori K, Mukoyama M, Nishiyama A. Reduction of Tubular Flow Rate as a Mechanism of Oliguria in the Early Phase of Endotoxemia Revealed by Intravital Imaging. J Am Soc Nephrol. 2015; 26:3035–44. [PubMed: 25855781]

Nakano D, Kobori H, Burford JL, Gevorgyan H, Seidel S, Hitomi H, Nishiyama A, Peti-Peterdi J. Multiphoton imaging of the glomerular permeability of angiotensinogen. J Am Soc Nephrol. 2012; 23:1847–56. [PubMed: 22997258]

Nguyen QT, Callamaras N, Hsieh C, Parker I. Construction of a two-photon microscope for video-rate Ca(2+) imaging. Cell Calcium. 2001; 30:383–393. [PubMed: 11728133]

Niesner R, Andresen V, Neumann J, Spiecker H, Gunzer M. The power of single and multibeam two-photon microscopy for high-resolution and high-speed deep tissue and intravital imaging. Biophys J. 2007; 93:2519–29. [PubMed: 17557785]

Ogasawara Y, Takehara K, Yamamoto T, Hashimoto R, Nakamoto H, Kajiya F. Quantitative blood velocity mapping in glomerular capillaries by *in vivo* observation with an intravital videomicroscope. Methods Inf Med. 2000; 39:175–178. [PubMed: 10892258]

Okada T, Takahashi S, Ishida A, Ishigame H. *In vivo* multiphoton imaging of immune cell dynamics. Pflugers Arch. 2016; 468:1793–1801. [PubMed: 27659161]

Peti-Peterdi J, Burford JL, Hackl MJ. The first decade of using multiphoton microscopy for high-power kidney imaging. Am J Physiol Renal Physiol. 2012; 302:F227–33. [PubMed: 22031850]

Rosivall L, Mirzahosseini S, Toma I, Sipos A, Peti-Peterdi J. Fluid flow in the juxtaglomerular interstitium visualized *in vivo*. Am J Physiol Renal Physiol. 2006; 291:F1241–F1247. [PubMed: 16868308]

Russo LM, Sandoval RM, McKee M, Osicka TM, Collins AB, Brown D, Molitoris BA, Comper WD. The normal kidney filters nephrotic levels of albumin retrieved by proximal tubule cells: Retrieval is disrupted in nephrotic states. Kidney Int. 2007; 71:504–513. [PubMed: 17228368]

Sandoval RM, Kennedy MD, Low PS, Molitoris BA. Uptake and trafficking of fluorescent conjugates of folic acid in intact kidney determined using intravital two-photon microscopy. Am J Physiol Cell Physiol. 2004; 287:C517–C526. [PubMed: 15102609]

Sandoval RM, Molitoris BA. Quantifying glomerular permeability of fluorescent *macromolecules* using 2-photon microscopy in Munich Wistar rats. J Vis Exp. 2013

Sandoval RM, Molitoris BA. Letter to the editor: “Quantifying albumin permeability with multiphoton microscopy: why the difference?”. Am J Physiol Renal Physiol. 2014; 306:F1098–100. [PubMed: 24785957]

Sandoval RM, Wagner MC, Patel M, Campos-Bilderback SB, Rhodes GJ, Wang E, Wean S, Clendenon S, Molitoris BA. Multiple factors influence glomerular albumin permeability in rats. J Am Soc Nephrol. 2012; 23:447–57. [PubMed: 22223875]

Sandoval RM, Wang E, Molitoris BA. Finding the bottom and using it: Offsets and sensitivity in the detection of low intensity values *in vivo* with 2-photon microscopy. Intravital. 2014; 2

Schiessl IM, Castrop H. Angiotensin II AT2 receptor activation attenuates AT1 receptor-induced increases in the glomerular filtration of albumin: a multiphoton microscopy study. Am J Physiol Renal Physiol. 2013; 305:F1189–200. [PubMed: 23946289]

Schiessl IM, Castrop H. Deep insights: intravital imaging with two-photon microscopy. Pflugers Arch. 2016; 468(9):1505–1516. [PubMed: 27352273]

Schiessl IM, Hammer A, Kattler V, Gess B, Theilig F, Witzgall R, Castrop H. Intravital Imaging Reveals Angiotensin II-Induced Transcytosis of Albumin by Podocytes. J Am Soc Nephrol. 2016a; 27:731–44. [PubMed: 26116357]

Schiessl IM, Kattler V, Castrop H. *In vivo* visualization of the antialbuminuric effects of the angiotensin-converting enzyme inhibitor enalapril. J Pharmacol Exp Ther. 2015; 353:299–306. [PubMed: 25680709]

Sharfuddin AA, Sandoval RM, Berg DT, McDougal GE, Campos SB, Phillips CL, Jones BE, Gupta A, Grinnell BW, Molitoris BA. Soluble thrombomodulin protects ischemic kidneys. J Am Soc Nephrol. 2009; 20:524–34. [PubMed: 19176699]

Squirrell JM, Wokosin DL, White JG, Bavister BD. Long-term two-photon fluorescence imaging of mammalian embryos without compromising viability. Nat Biotechnol. 1999; 17:763–767. [PubMed: 10429240]

Steinhausen M, Tanner GA. Microcirculation and tubular urine flow in the mammalian kidney cortex (*in vivo* microscopy). Sitzungsberichte Heidelberger Akad Wissensch Math-naturwissensch Kl. 1976; 3:279–335.

Steinhausen M, Eisenbach GM, Bottcher W. High-frequency microcinematographic measurements on peritubular blood flow under control conditions and after temporary ischemia of rat kidneys. Pflugers Arch. 1973; 339:273–288. [PubMed: 4735609]

Sutton TA, Mang HE, Campos SB, Sandoval RM, Yoder MC, Molitoris BA. Injury of the renal microvascular endothelium alters barrier function after ischemia. Am J Physiol Renal Physiol. 2003; 285:F191–F198. [PubMed: 12684225]

Sutton TA, Kelly KJ, Mang HE, Plotkin Z, Sandoval RM, Dagher PC. Minocycline reduces renal microvascular leakage in a rat model of ischemic renal injury. Am J Physiol Renal Physiol. 2005; 288:F91–F97. [PubMed: 15353401]

Svoboda K, Denk W, Kleinfeld D, Tank DW. *In vivo* dendritic calcium dynamics in neocortical pyramidal neurons. Nature. 1997; 385:161–165. [PubMed: 8990119]

Tanner GA, Sandoval RM, Dunn KW. Two-photon *in vivo* microscopy of sulfonefluorescein secretion in normal and cystic rat kidneys. Am J Physiol Renal Physiol. 2004; 286:F152–F160. [PubMed: 12965895]

Toma I, Kang JJ, Peti-Peterdi J. Imaging renin content and release in the living kidney. Nephron Physiol. 2006; 103:71–74.

Wagner MC, Campos-Bilderback SB, Chowdhury M, Flores B, Lai X, Myslinski J, Pandit S, Sandoval RM, Wean SE, Wei Y, Satlin LM, Wiggins RC, Witzmann FA, Molitoris BA. Proximal Tubules Have the Capacity to Regulate Uptake of Albumin. J Am Soc Nephrol. 2016; 27:482–94. [PubMed: 26054544]

Weigert R, Sramkova M, Parente L, Amornphimoltham P, Masedunskas A. Intravital microscopy: a novel tool to study cell biology in living animals. Histochem Cell Biol. 2010; 133:481–91. [PubMed: 20372919]

Winfree S, Khan S, Micanovic R, Eadon MT, Kelly KJ, Sutton TA, Phillips CL, Dunn KW, El-Achkar TM. Quantitative Three-Dimensional Tissue Cytometry to Study Kidney Tissue and Resident Immune Cells. J Am Soc Nephrol. 2017; 28:2108–2118. [PubMed: 28154201]

Xu C, Williams RM, Zipfel W, Webb W. Multiphoton excitation cross-sections of molecular fluorophores. Bioimaging. 1996; 4:198–207.

Yamamoto T, Tada T, Brodsky SV, Tanaka H, Noiri E, Kajiya F, Goligorsky MS. Intravital videomicroscopy of peritubular capillaries in renal ischemia. Am J Physiol Renal Physiol. 2002; 282:1150–1155.

Yatim KM, Gosto M, Humar R, Williams AL, Oberbarnscheidt MH. Renal dendritic cells sample blood-borne antigen and guide T-cell migration to the kidney by means of intravascular processes. Kidney Int. 2016; 90:818–27. [PubMed: 27528552]

Yu W, Sandoval RM, Molitoris BA. Quantitative intravital microscopy using a Generalized Polarity concept for kidney studies. Am J Physiol Cell Physiol. 2005; 289:1197–1208.

Yu W, Sandoval RM, Molitoris BA. Rapid determination of renal filtration function using an optical ratiometric imaging approach. Am J Physiol Renal Physiol. 2007; 292:F1873–80. [PubMed: 17311910]

Zipfel WR, Williams RM, Webb WW. Nonlinear magic: Multiphoton microscopy in the biosciences. Nat Biotechnol. 2003; 21:1369–1377. [PubMed: 14595365]

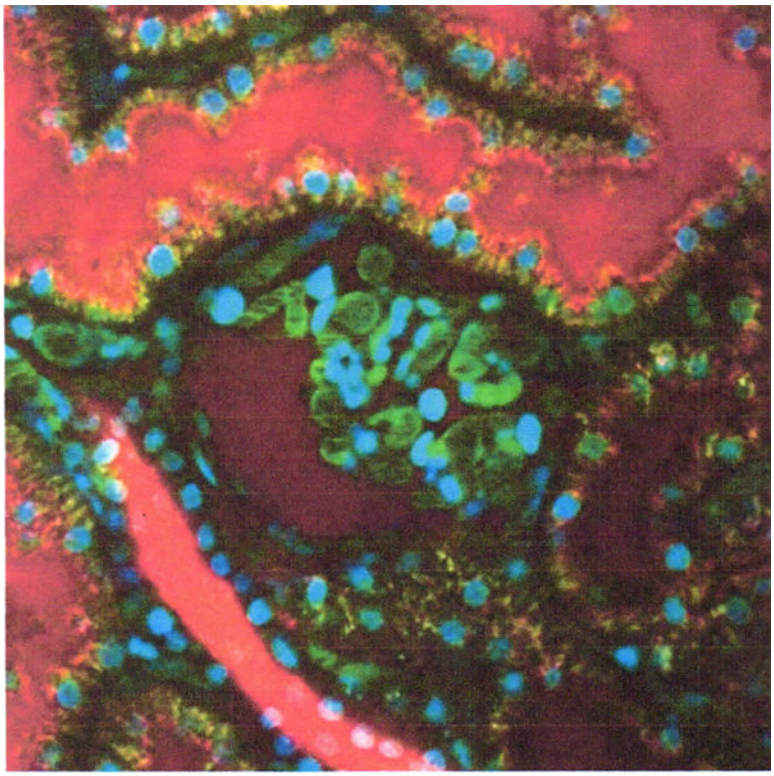

Figure 1.

Intravital assay of glomerular permeability. This figure shows a multiphoton fluorescence optical section of the kidney of a living rat injected with Hoechst 33342 to label nuclei (blue), a 500-Kda dextran–Alexa 488 (green) that is retained in the vasculature, and a 5-Kda dextran-rhodamine (red) that is rapidly filtered, appearing first in the Bowman's space (center), then in the proximal tubules (top), and finally concentrating in the distal tubules (bottom left). The field of view is 200 μm across. For color version of this figure see http://www.currentprotocols.com.

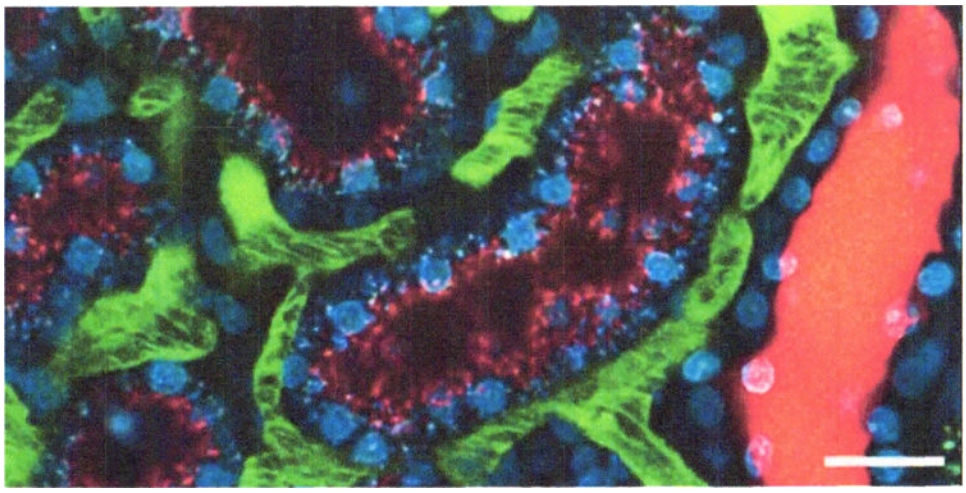

Figure 2.

Intravital assay of proximal tubule endocytosis. This figure shows a projection of multiphoton fluorescence images of the kidney of a living rat injected with Hoechst 33342 and a 3000-Da dextran–Cascade Blue, and then with a 3000-Da dextran–Texas Red 1 hr later. The image shown was collected 10 min following injection of the dextran-Texas Red. In this image, the Texas Red–dextran has progressed only as far as early endosomes, distributed in the apex of the proximal tubule cells (red puncta), whereas the Cascade Blue–dextran is seen in distinct, basally localized compartments, reflecting the progression of this probe into later endocytic and lysosomal compartments. Note the absence of endocytic uptake by the epithelial cells of the distal tubule on the right. Scale bar is 20 μm. For color version of this figure see http://www.currentprotocols.com.

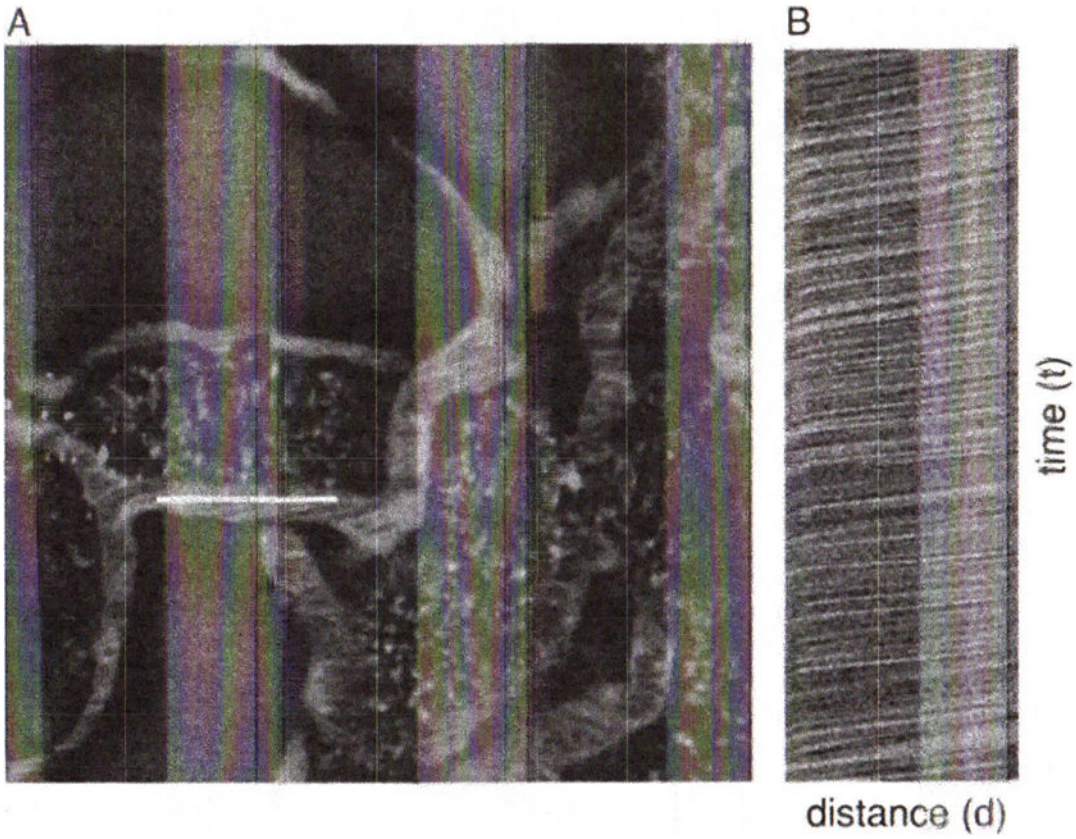

Figure 3.

Measurement of microvascular blood flow. Rhodamine-labeled albumin was infused by bolus injection into the jugular vein of an animal and an area of interest in the kidney was imaged by multiphoton microscopy. (**A**) A line scan was performed along the central axis of the vessel of interest (white line) continuously at a rate of 2 msec per line for 1 sec (500 lines total). Flowing red blood cells, which exclude the fluorescent probe, appear as black objects. (**B**) The line scans were combined into a single image in B, resulting in an image in which the vertical axis represents time (the 1-sec interval of line-scan collection), and the horizontal axis represents distance (the length of the scan). Thus the dark lines in panel B reflect the passage of blood cells along the linescan over time, and the velocity of each can be determined by measuring the slope of the line $(\Delta d/\Delta t)$ as described by Kang et al. (2006). Field of view is 70 μm across.

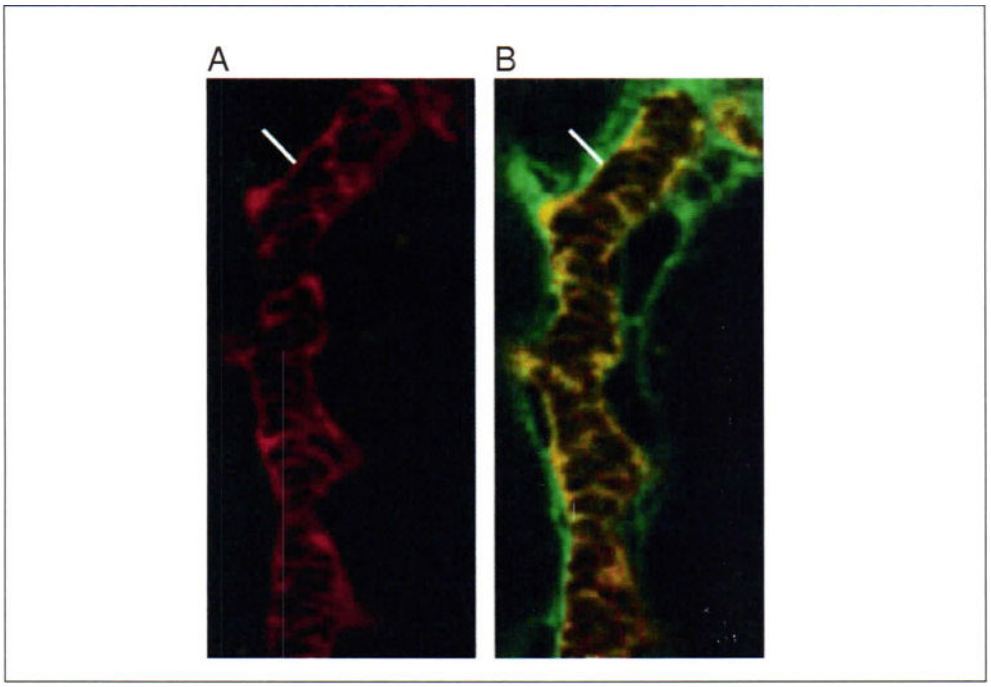

Figure 4.

Measurement of vascular permeability. (**A**) A rhodamine-labeled (red) dextran (500,000 Da) was infused by bolus injection into the jugular vein of an animal and a renal microvessel of interest was imaged by multiphoton microscopy to determine the vascular space. This was followed by the bolus injection of a fluorescein (green)-dextran (10,000 Da). The vessel of interest was imaged every 0.45 sec after injection of the fluorescein-dextran. (**B**) Representative image from this time series. The permeability of the vessel can be measured by integrating the fluorescence intensity along a line perpendicular to the vessel as described by Brown et al. (2001). Indicated lines reflect a distance of 3 μm. For color version of this figure see http://www.currentprotocols.com.

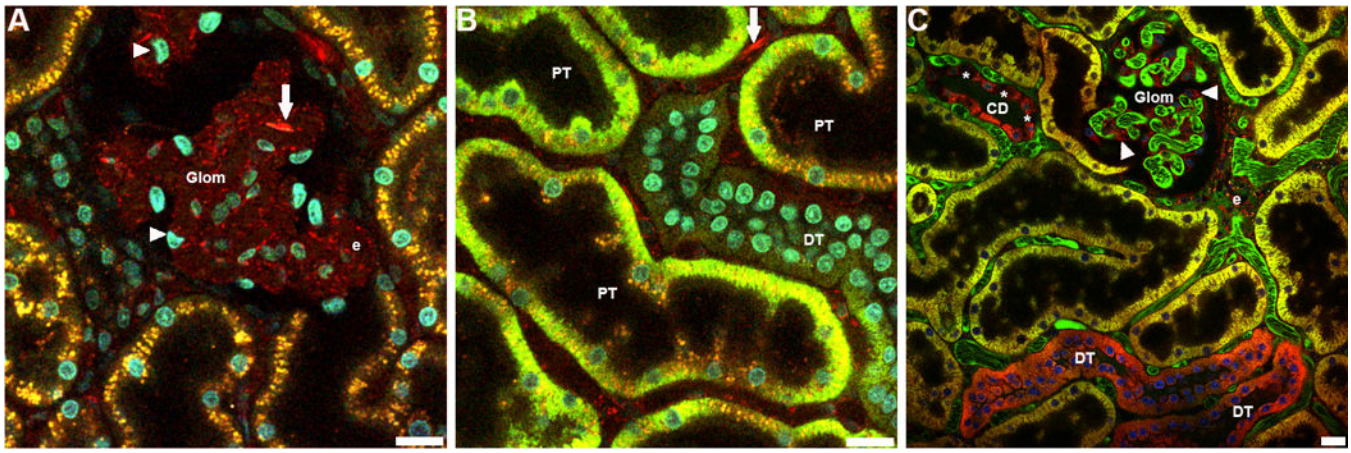

Figure 5.

Intravital assay of mitochondrial function. Mitochondria in the kidney of a living rat were labeled by sequential intravenous injection of rhodamine B hexyl ester, rhodamine 123 and Tetramethylrhodamine methyl ester. Accordingly, panel A shows the distribution of rhodamine B hexyl ester, panel B shows the distribution of rhodamine B hexyl ester and rhodamine 123 and panel C shows the distribution of all three probes. (**A**) Rhodamine B hexyl ester (red) accumulates in mitochondria of podocytes surrounding the glomerular capillary loops (Glom, arrowheads), circulating white blood cells (WBCs, arrows) and vascular endothelial cells (e). (**B**) Rhodamine 123 (green) accumulates mainly in mitochondria of proximal tubule cells (PTs), with some very faint accumulation occurring within the mitochondria of distal tubules (DTs). This image demonstrates the heterogeneity of mitochondrial potential within PTs during the loading process. Cells within the tubule having a higher mitochondrial potential will accumulate the dye more readily than neighboring cells with lower potentials. Note the single WBC in the field labeled with Rhodamine B hexyl ester (red, indicated with arrow). (**C**) Tetramethylrhodamine methyl ester perchlorate (TMRM, red) accumulates in mitochondria of distal tubules (DTs) and the mitochondria of principal cells in collecting ducts (CD). Intercalated cells (asterisks) exclude the dye giving the tubule a checkerboard accumulation pattern. For this image, a large 150kDa fluorescein dextran (green) was also introduced to label the peritubular microvasculature and glomerular capillary loops (Glom). Note the mitochondria of podocytes labeled with rhodamine B hexyl ester (arrowheads) surrounding the capillary loops. All panels labeled with Hoechst 33342 (blue/cyan); bar = 20μm.

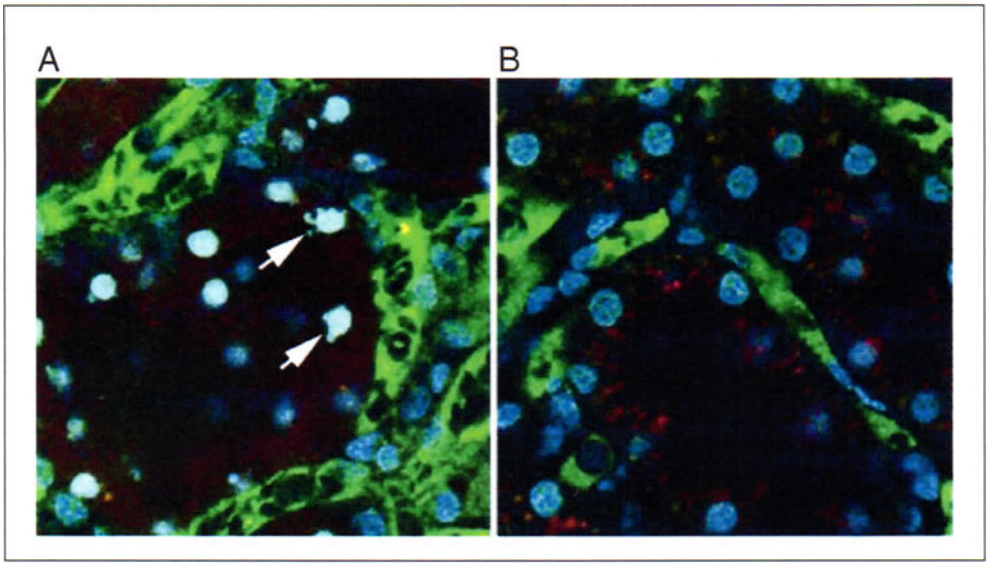

Figure 6.

Apoptosis and necrosis. Apoptotic cells can be identified by their characteristically fragmented nuclear morphology, using Hoechst 33342 to fluorescently label nuclei. (**A**) Optical section collected from a living rat previously given a cecal ligation and puncture injury. This animal was injected with Hoechst, as well as a large green dextran (labeling vasculature) and a small red dextran (labeling tubule lumens and endosomes). Arrows indicate a few of the apoptotic tubular cells imaged in this field. (**B**) Corresponding image from an untreated animal. The nuclei in this image are characteristically regular in shape, and labeled less intensely with Hoechst 33342. Fields are 100 μm in diameter. For color version of this figure see http://www.currentprotocols.com.

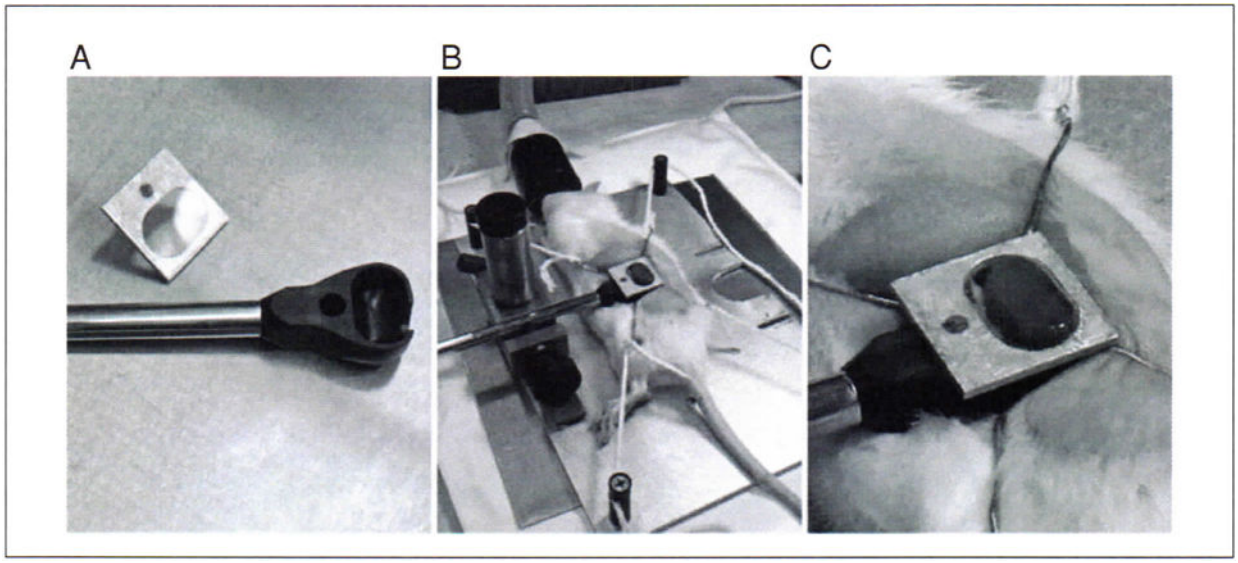

Figure 7.

In order to image the kidney of a living animal with an upright microscope, the kidney must be supported in a kidney cup. The kidney cup can be fashioned out thin plastic or metal. It is critical that the cup be small enough to fit within the animal and positioned around the kidney in such a way that blood flow to the kidney is not significantly altered (i.e., by placing excessive tension on the renal pedicle). (**A**) The kidney cup (black) is mounted on a support rod. A coverglass, mounted on an aluminum bracket, is attached to the top of the cup, after insertion of the kidney. (**B**) Following surgery, the kidney of a living rat is placed into the kidney cup, whose support rod is attached to an adjustable support structure. (**C**) Close-up of the kidney cup in position.

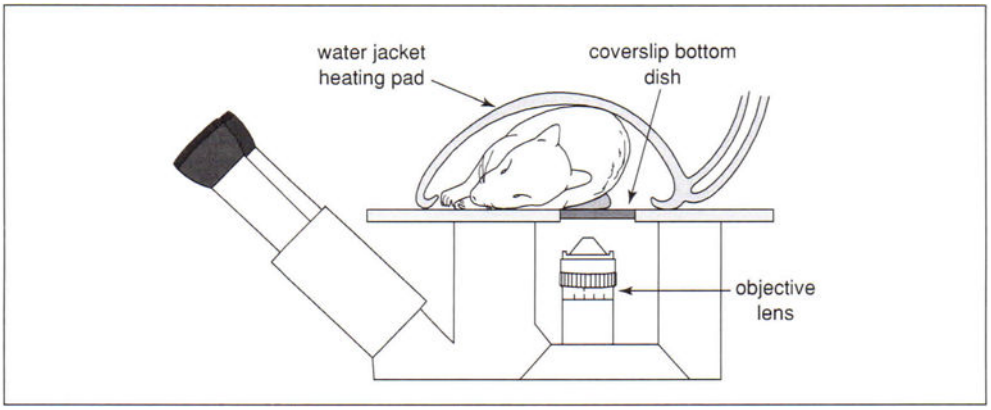

Figure 8.

A schematic diagram of the arrangement for imaging a living rodent on an inverted microscope. The kidney of a living rat or mouse can be imaged on an inverted microscope stand by placing the kidney into an isotonic saline–filled 50-mm cell-culture dish whose bottom has been replaced with a No. 1.5 coverslip. As shown, the rat lies on its side on a heated microscope stage, wrapped in a heating pad. (Two Repti-Therm heating pads placed beneath the head and legs are not shown). The kidney is thus gently pressed against the coverslip, so that it may be imaged by the objective located below the microscope stage.

Table 12.9.1

Probe Types and Characteristics

Probe	Characteristic
Hoecsht 33342	A cyan-fluorescing, DNA-binding probe. Membrane-permeant, it labels nuclei of all cells; especially useful in assays of apoptosis. It has a wide emission spectra that will bleed into green channels with multi-photon excitation
Propidium iodide	A red-fluorescing, DNA-binding probe. Membrane-impermeant, it labels the nuclei of necrotic cells.
3,000-Da dextran[a]	A bulk probe that, when injected intravenously, is freely filtered by the glomerulus. Used for assays of glomerular permeability and proximal tubule endocytosis.
10,000-Da dextran[a]	A bulk probe that, when injected intravenously, is freely filtered by the glomerulus, and is permeant in the vasculature. Used for assays of glomerular permeability, proximal tubule endocytosis, and vascular permeability.
40,000-Da dextran[a]	A bulk probe that, when injected intravenously, is slowly filtered by the kidney, and is relatively impermeant in the vasculature to extravasation into the interstitial space. Used for assays of glomerular permeability, vascular flow, and vascular permeability.
150,000-Da dextran[a]	A bulk probe that when injected intravenously, is not filtered by the kidney, but is retained in the vasculature. Used for assays of glomerular permeability, vascular flow, and vascular permeability
500,000-Da dextran[a]	A bulk probe that, when injected intravenously, is not filtered by the kidney, but is retained in the vasculature. Used for assays of glomerular permeability, vascular flow, and vascular permeability.
Serum Albumin[a]	A bulk probe that, when injected intravenously, is very slowly filtered by the kidney. Used for assays of glomerular permeability, proximal tubule endocytosis, vascular flow, and vascular permeability.
Rhodamine B hexyl ester	A red-fluorescing probe that accumulates in mitochondria, on the basis of membrane potential. Injected intravenously, it labels the mitochondria of metabolically active endothelial cells, circulating white blood cells, and podocytes surrounding glomerular capillary loops.
Rhodamine 123	A green-fluorescing mitochondrial probe that accumulates on the basis of membrane potential, injected intravenously. At lower concentrations it selectively accumulates in the mitochondria of proximal tubule cells.
Tetramethyl-rhodamine, Methyl Ester, Perchlorate (TMRM)	A red-fluorescing mitochondrial probe that accumulates on the basis of membrane potential, injected intravenously. At lower concentrations it selectively accumulates in the mitochondrial of distal tubule cells and principal cells of collecting ducts but not intercalated cells; producing a checkerboard pattern.

[a]Non-fluorescent probes that must be conjugated to fluorophore (see Reagents and Solutions section).